

Interaction-induced topological bound states and Thouless pumping in a one-dimensional optical lattice

Ling Lin^{1,2}, Yongguan Ke^{1,3}, and Chaohong Lee^{1,2,3,*}

¹Guangdong Provincial Key Laboratory of Quantum Metrology and Sensing & School of Physics and Astronomy, Sun Yat-Sen University (Zhuhai Campus), Zhuhai 519082, China

²State Key Laboratory of Optoelectronic Materials and Technologies, Sun Yat-Sen University (Guangzhou Campus), Guangzhou 510275, China

³Nonlinear Physics Centre, Research School of Physics, Australian National University, Canberra ACT 2601, Australia



(Received 22 October 2019; accepted 3 February 2020; published 27 February 2020)

We study topological features of interacting spin- $\frac{1}{2}$ particles in one-dimensional state-dependent optical lattices. Due to the cotranslational symmetry, we introduce the center-of-mass Zak phase with the help of center-of-mass momentum. There appear topological bound states composed by two particles in different spin states via tuning hopping and interaction strengths. Under symmetric open boundary conditions, topological edge bound states appear as a result of the nontrivial center-of-mass Zak phase of bound-state band, which is protected by the center-of-mass inversion symmetry. The interaction plays a crucial role in the appearance of topological bound states and the system becomes completely trivial if the interaction is switched off. By periodically modulating the hopping and interaction strengths, we show how to implement topological Thouless pumping of bound states, in which the quantized shift of center of mass can be described by a nontrivial center-of-mass Chern number.

DOI: [10.1103/PhysRevA.101.023620](https://doi.org/10.1103/PhysRevA.101.023620)

I. INTRODUCTION

Topological band theory provides a general framework to explain topological features via topological invariants defined with single-particle energy bands. It can be traced back to the great success in explaining quantum Hall effects (QHE) [1], in which a so-called TKNN invariant (i.e., Chern number) is used to distinguish different phases of matters. Topological phase transitions happen when topological invariants change. Later on, Chern number was linked to the quantized charge pumping in one-dimensional (1D) periodically modulated lattices [2], which has the same origin as QHE. For decades, topological band theory played a key role in identifying topological states and exploring topological materials [3–7].

Ultracold atomic systems have been proved as a powerful platform for the investigation of noninteracting topological states, i.e., the realization of Thouless pumping [8,9], Hofstadter model [10] and Haldane model [11], measurement of Zak phase [12], dynamical characterization of topological phases [13,14], etc. The experimental realizations of the spin-orbit couplings in ultracold atomic gases [15–17] also bring a new approach to topological states. Because the interactions between atoms can be precisely tuned by Feshbach resonances, there are increasing interests in the interplay between interaction and topology in ultracold atom systems [18,19]. Recently, it has been reported that the symmetry-protected topological phase is observed with interacting Rydberg atoms [20].

It is challenging to study the topology in a general interacting many-body system, since conventional topological band theory fails as the interparticle interaction breaks the single-particle translation symmetry. To overcome this problem, a method based on twisted boundary condition (TBC) has been utilized to analyze the many-body topological effects [21]. Another alternative method is the generalized topological band theory regarding the center-of-mass (c.m.) momentum [22,23]. Due to strong interaction, the bands of the bound states are isolated from the continuum band [24–27]. Such bound states have experimentally demonstrated to be stable even if the interaction is repulsive [28]. In recent years, topological bound states have been found in various systems, such as Su-Schrieffer-Heeger (SSH) model [29–32], XXZ chain [33], Haldane model [34], Hofstadter superlattice model [23], Rice-Mele model [22], and Floquet system [35]. Among these models, we note that they may support topological states even in the absence of interaction. A natural question arises: are there topological states in an interacting multiparticle system whose noninteracting counterpart does not support any topological state? Furthermore, due to the interaction, some discrete symmetries essential to topology are reduced, such as chiral symmetry and inversion symmetry. Therefore, we are wondering if any essential discrete symmetry is still preserved in 1D interacting systems.

In this work, we study interacting spin- $1/2$ particles in a one-dimensional state-dependent lattice, in which the hopping strengths are state dependent and interaction strengths are distancedependent. We first calculate the two-particle energy bands with respect to c.m. momentum. We find the existence of interaction-induced topological bound states which are

*lichao2@mail.sysu.edu.cn; chleeen@gmail.com

characterized by c.m. Zak phase. Remarkably, the topological bound states are protected by the c.m. inversion symmetry, and the c.m. Zak phase is quantized if the interspecies interactions are the same. The topological edge bound states under open boundary conditions are supported by nontrivial two-body Zak phases, indicating the existence of bulk-boundary correspondence in the interacting systems. Moreover, we propose a scheme of implementing topological Thouless pumping via modulating the interactions and tunnelings. The nontrivial c.m. Chern number indicates a quantized shift of c.m. position, which is verified by our numerical simulation. We emphasize that both the topological bound state and the topological transport are completely induced by interaction effects.

The paper is organized as follows. In Sec. II A, we introduce the c.m. Zak phase and Chern number based upon the c.m. momentum. In Sec. II B, we describe our two-particle system in a 1D state-dependent optical lattice. In Sec. II C, we calculate the Bloch Hamiltonian and give the energy band structure with respect to the c.m. momentum. In Sec. II D, we investigate the topology of the isolated bands with the help of c.m. Zak phase. In Sec. III, we propose a scheme to implement the interaction-induced topological Thouless pumping. Finally, we give a summary and discuss our results in Sec. IV.

II. COTRANSLATIONAL SYMMETRY AND CENTER-OF-MASS ZAK PHASE

A. General formalism

For an interacting system under the periodic boundary condition (PBC), the quasimomentum of single particle is no longer the conserved quantity. Considering interaction that only depends on relative position between particles, the Hamiltonian

$$H = H_T + V = \sum_i H_{T,i} + \sum_{i<j} V(|r_i - r_j|) \quad (1)$$

is invariant under the cotranslation of all N particles through a unit cell in one-dimensional lattice with periodic boundary condition [23,33]. For simplicity, we consider a normal 1D lattice with N particles and L sites here. The cotranslation operation is formulated by

$$\hat{T}|r_1, r_2, \dots, r_N\rangle = |r_1 + 1, r_2 + 1, \dots, r_N + 1\rangle, \quad (2)$$

where \hat{T} is the cotranslation operator and r_n , $n = 1, 2, \dots, N$ denotes the position of the n th particle. The lattice constant is set to unity $a = 1$ by default. With the cotranslation symmetry, one has $[\hat{H}, \hat{T}] = 0$. The corresponding conserved quantity is the center-of-mass (c.m.) quasimomentum K of all particles.

Before proceeding further, we introduce the concept of *seed basis* [22]. Generally speaking, the seed basis is all the possible states that *cannot* be generated to each other by cotranslation operator \hat{T} . The total number of the seed basis depends on the number of particles and the geometry of lattice. Physically, each element of the seed basis corresponds to a certain distribution of particles, and we shall denote this set as $\{|r_1, \dots, r_N\rangle\}$. The choice of seed basis seems to be somewhat arbitrary. For example, given a certain particle distribution r_1, \dots, r_N , one can choose either $|r_1, \dots, r_N\rangle$ or

$|r_1 + d, \dots, r_N + d\rangle$, $d \in \mathbb{Z}$ as one of the seed basis. In fact, different choices of seed basis correspond to different *gauge* choices for $|K, \alpha\rangle$ [36]. Although the choice of gauge does not affect the energy bands, it may affect the calculation of Berry phase. We would like to remark that different elements of the seed basis can be considered as different virtual ‘‘orbits’’ labeled by α . In this angle, the many-body system can be considered as a single quasiparticle. Thus the generalization from band theory of a single particle to the many-body case is quite natural and reasonable.

Eigenstates of cotranslation operator \hat{T} are found to be the superposition of a series state generated by any of the given seed basis

$$\begin{aligned} |K, \alpha\rangle &= \frac{1}{\sqrt{L}} \sum_{l=0}^{L-1} e^{iK(l+\sum_i r_i/N)} \hat{T}^l |\{r_\alpha\}\rangle \\ &= \frac{1}{\sqrt{L}} \sum_{l=0}^{L-1} e^{iK(l+\sum_i r_i/N)} |\{r_\alpha\} + l\rangle, \end{aligned} \quad (3)$$

where $|\{r_\alpha\} + l\rangle \equiv |r_1 + l, r_2 + l, \dots, r_N + l\rangle$ and $\{r_\alpha\}$ denotes one of the given seed basis $|r_1, r_2, \dots, r_N\rangle$, which is characterized by α . The eigenvalues of \hat{T} can be derived as

$$\begin{aligned} \hat{T}|K, \alpha\rangle &= \sum_l e^{iK(l+\sum_i r_i/N)} \hat{T} |r_1 + l, \dots, r_N + l\rangle \\ &= \sum_l e^{iK(l+\sum_i r_i/N)} |r_1 + (l+1), \dots, r_N + (l+1)\rangle \\ &= e^{-iK} \sum_l e^{iK(l+1+\sum_i r_i/N)} |r_1 + (l+1), \dots, (r_N + l+1)\rangle \\ &= e^{-iK} |K, \alpha\rangle. \end{aligned} \quad (4)$$

For a lattice with PBC, there is $r_n + L = r_n$, and therefore \hat{T}^L is an identity matrix, yielding $e^{-iLK} = 1$, $K = 2\pi n/L$, $n \in \mathbb{Z}$.

The Hamiltonian can be block diagonalized as the summation of Bloch Hamiltonians with momentum K ,

$$\hat{H} = \oplus_K \hat{H}(K), \quad (5)$$

where

$$H_{\alpha',\alpha}(K) = \langle K, \alpha' | \hat{H} | K, \alpha \rangle. \quad (6)$$

The eigenstates of $\hat{H}(K)$ are the linear combinations of seed basis

$$|\psi_K^n\rangle = \sum_{\{\alpha\}} u_{K,\alpha}^n |K, \alpha\rangle, \quad (7)$$

in which $\{\alpha\}$ implies the summation of $|K, \alpha\rangle$ with respect to all seed basis labeled by α . By solving the eigenvalue problem of $H(K)$, one can obtain the eigenvectors $u_{K,\alpha}^n$ and eigenvalues E_K^n .

The Brillouin zone (BZ) with respect to c.m. momentum K forms a manifold; it is natural to investigate the topology of this manifold. Here, with respect to the c.m. momentum, we introduce the concepts of c.m. Zak phase [37]

$$\gamma_{\text{Zak}}^n = i \int_{-\pi}^{\pi} \langle u_K^n | \partial_K | u_K^n \rangle dK \quad (8)$$

for a 1D system (we mention it as Zak phase for short in the following), and c.m. Chern number [22]

$$C_n = \frac{i}{2\pi} \int_{BZ} dK \int_0^T dt (\langle \partial_t u_K^n | \partial_K u_K^n \rangle - \langle \partial_K u_K^n | \partial_t u_K^n \rangle) \quad (9)$$

for a (1+1)D system where the Hamiltonian is periodically modulated with period T . This is quite similar to the well-known topological band theory in a noninteracting system.

It has been shown that the c.m. shift of the multiparticle Wannier state is related to the c.m. Chern number [22] in the topological pumping process. It is tempting to investigate the physical interpretation of the c.m. Zak phase. According to the modern theory of polarization, it is known that the Zak phase in the noninteracting case is related to the Wannier center (or band center [37,38]) within the unit cell [39,40]. Next, we will use a similar method to show explicitly that the c.m. Zak phase is related to the c.m. position.

First, the multiparticle Wannier function centered at R_0 for an isolated band can be defined as

$$|w_n(R_0)\rangle = \frac{1}{\sqrt{L}} \sum_K e^{-iKR_0} |\psi_K^n\rangle, \quad (10)$$

where $|\psi_K^n\rangle$ is the many-body Bloch state with respect to the c.m. momentum introduced in Eq. (7). Next, we introduce the c.m. position operator \hat{R} such that $\hat{R}|r_1, r_2, \dots, r_N\rangle = (\sum_i r_i/N)|r_1, r_2, \dots, r_N\rangle$. Then we would like to calculate the expectation value of \hat{R} with respect to $|w_n(R_0)\rangle$

$$\begin{aligned} \langle \hat{R} \rangle_w &= \langle w_n(R_0) | \hat{R} | w_n(R_0) \rangle \\ &= \frac{1}{L} \sum_{K, K'} e^{-i(K-K')R_0} \langle \psi_{K'}^n | \hat{R} | \psi_K^n \rangle. \end{aligned} \quad (11)$$

To calculate $\langle \psi_{K'}^n | \hat{R} | \psi_K^n \rangle$, we adopt the argument in Ref. [41], where the average position $\langle x \rangle$ of the extended wave function under the PBC should be calculated as

$$\langle x \rangle = \frac{L}{2\pi} \text{Im}[\log \langle \psi | e^{i\delta K \hat{x}} | \psi \rangle], \quad (12)$$

in which $\delta K = 2\pi/L$. Therefore, the matrix element $\langle \psi_{K'}^n | \hat{R} | \psi_K^n \rangle$ should be modified as $\langle \psi_{K'}^n | \hat{R} | \psi_K^n \rangle = \frac{L}{2\pi} \text{Im}[\log \langle \psi_{K'}^n | e^{i\frac{2\pi}{L} \hat{R}} | \psi_K^n \rangle]$. With some algebraic calculations, one has

$$\begin{aligned} \langle \psi_{K'}^n | e^{i\frac{2\pi}{L} \hat{R}} | \psi_K^n \rangle &= \frac{1}{L} \sum_{l, l'} e^{i(Kl-K'l')} \sum_{\alpha, \alpha'} (u_{K', \alpha'}^{n*} u_{K, \alpha}^n e^{i(K \sum_i r_i - K' \sum_i r'_i)/N} \{r_{\alpha'}\} \\ &\quad + l' | e^{i\delta K \hat{R}} | \{r_{\alpha}\} + l) \\ &= \frac{1}{L} \sum_{l, l'} e^{i(Kl-K'l')} \sum_{\alpha, \alpha'} e^{i\delta K(l + \sum_i r_i/N)} \\ &\quad \times e^{i(K \sum_i r_i - K' \sum_i r'_i)/N} u_{K', \alpha'}^{n*} u_{K, \alpha}^n \delta_{l, l'} \delta_{\alpha, \alpha'} \\ &= \frac{1}{L} \sum_{\alpha} u_{K', \alpha}^{n*} u_{K, \alpha}^n \sum_l e^{i(K-K'+\delta K)(l + \sum_i r_i/N)} \\ &= \delta_{K', K+\delta K} \sum_{\alpha} u_{K', \alpha}^{n*} u_{K, \alpha}^n, \end{aligned} \quad (13)$$

in which $\sum_i r_i$ is the summation of positions of all particles. Combining Eqs. (11) and (13), one obtains

$$\begin{aligned} \langle \hat{R} \rangle_w &= \sum_K \frac{1}{2\pi} \text{Im} \left[\log \left(e^{i\delta K R_0} \sum_{\alpha} u_{K+\delta K, \alpha}^{n*} u_{K, \alpha}^n \right) \right] \\ &= R_0 + \frac{1}{2\pi} \text{Im} \left[\sum_K \log \langle u_{K+\delta K}^n | u_K^n \rangle \right], \end{aligned} \quad (14)$$

in which we have used a compact notation $|u_K^n\rangle$, according to $\hat{H}(K)|u_K^n\rangle = E_K^n|u_K^n\rangle$. Note that, up to first order, there is $|u_{K+\delta K}^n\rangle \approx |u_K^n\rangle + \partial_K |u_K^n\rangle \delta K$. Therefore, we have

$$\langle u_{K+\delta K}^n | u_K^n \rangle \approx 1 + \langle \partial_K u_K^n | u_K^n \rangle \delta K. \quad (15)$$

Using the relation $\log(1+x) \approx x$ for $x \rightarrow 0$, we can write Eq. (14) as

$$\begin{aligned} \langle \hat{R} \rangle_w &\approx R_0 + \frac{1}{2\pi} \text{Im} \left[\sum_K \log (1 + \langle \partial_K u_K^n | u_K^n \rangle \delta K) \right] \\ &\approx R_0 + \frac{1}{2\pi} \text{Im} \sum_K \langle \partial_K u_K^n | u_K^n \rangle \delta K \\ &= R_0 + \frac{i}{2\pi} \sum_K \langle u_K^n | \partial_K | u_K^n \rangle \delta K, \end{aligned} \quad (16)$$

in which we have used the fact that $\langle \partial_K u_K^n | u_K^n \rangle$ is a purely imaginary quantity so that $\langle \partial_K u_K^n | u_K^n \rangle = -\langle u_K^n | \partial_K | u_K^n \rangle$. In the thermodynamic limit $L \rightarrow \infty$, the summation Eq. (16) becomes integral:

$$\langle \hat{R} \rangle_w = R_0 + \frac{i}{2\pi} \int_{-\pi}^{\pi} \langle u_K^n | \partial_K | u_K^n \rangle dK = R_0 + \frac{\gamma_{\text{Zak}}^n}{2\pi}. \quad (17)$$

Therefore, we know that the c.m. Zak phase is related to the c.m. position of multiparticle Wannier states. The result can be also generalized to a 1D superlattice or model in higher dimension.

B. Model

With the theory of describing the many-body topological properties in hand, we would like to explore the existence of interaction-induced topological states. We consider two spin-1/2 particles trapped by a state-dependent optical lattice [42–45]. The state-dependent lattice considered here consists of two lattices, which have the same periodicity but different phase $\Delta\phi$. These two different particles are trapped separately. The phase difference between two lattices indicates they have a relative spatial shift in real space, as shown in Fig. 1. The Hamiltonian of this system can be written as

$$\begin{aligned} \hat{H} &= - \sum_{l, \sigma=\uparrow, \downarrow} (J_{\sigma} \hat{c}_{\sigma, l}^{\dagger} \hat{c}_{\sigma, l+1} + \text{H.c.}) \\ &\quad + \sum_l (V_1 \hat{n}_{\downarrow, l} \hat{n}_{\uparrow, l} + V_2 \hat{n}_{\downarrow, l+1} \hat{n}_{\uparrow, l}), \end{aligned} \quad (18)$$

where $\hat{c}_{\sigma, l}^{\dagger}$ and $\hat{c}_{\sigma, l}$ are respectively the creation and annihilation operators of spin- σ particles in the l th site ($\sigma = \uparrow, \downarrow$, $l = 1, 2, \dots, L$). We suppose there are only the intraspecies tunnelings J_{σ} , and the interspecies tunnelings (spin flip) are

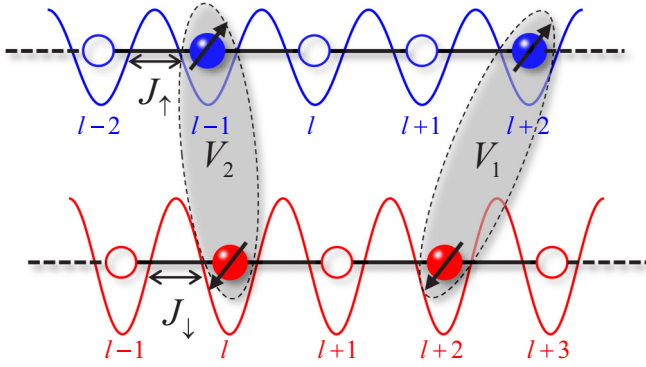


FIG. 1. Sketch for 1D state-dependent lattice where two kinds of spin-1/2 particles are trapped separately. The phases of two periodic lattices have relative spatial shift. Blue and red lattices represent the periodic potential for spin-up and spin-down particles, respectively. Arrows represent the NN tunneling. Gray shadings represent the NN interspecies interaction. The two lattices are overlapped in real space. The labels of sites is shown, and we will adapt this convention of labeling the sites in this work.

forbidden. Thus the particle number of each species is conserved. Furthermore, we assume nearest-neighbor (NN) interspecies interaction between spin-up and spin-down particles is present. The interaction strength will depend on the relative distance between the particles (see Appendix. A for detailed discussions), and can be tuned via Feshbach resonance [46]. As the two lattices have relative shift, there are two kinds of NN interaction strengths $V_{1,2}$, as depicted by the gray-dashed lines in Fig. 1. Without loss of generality, the interaction is assumed to be repulsive ($V_{1,2} > 0$) by default in the following context.

$$H(K) = \begin{bmatrix} V_2 & -(J_\downarrow + J_\uparrow e^{-iK}) & 0 & \cdots & -(J_\downarrow + J_\uparrow e^{iK}) \\ -(J_\downarrow + J_\uparrow e^{iK}) & 0 & -(J_\downarrow + J_\uparrow e^{-iK}) & \cdots & 0 \\ 0 & -(J_\downarrow + J_\uparrow e^{iK}) & \ddots & \cdots & \vdots \\ \vdots & \vdots & \vdots & 0 & -(J_\downarrow + J_\uparrow e^{-iK}) \\ -(J_\downarrow + J_\uparrow e^{-iK}) & 0 & 0 & -(J_\downarrow + J_\uparrow e^{iK}) & V_1 \end{bmatrix}. \quad (22)$$

By numerically diagonalizing the Bloch Hamiltonian Eq. (22) for all c.m. quasimomentum K , we obtain the energy bands of the system within the first Brillouin zone. In the noninteracting case, the system is simply the direct product of two normal lattices. Correspondingly, the c.m. quasimomentum is an average of two single-particle momentum $K = (k_\downarrow + k_\uparrow)/2$. The energy bands with respect to $K = (k_\downarrow + k_\uparrow)/2$ are shown in Fig. 2(a). For strong interaction, there appears one continuum and two isolated bands, as shown in Figs. 2(b)–2(d). The continuum corresponds to states in which two particles move quasi-independently. The isolated bands correspond to bound states, where particles are bound by interaction and perform correlated dynamics. The appearance of two isolated bands is because there are two kinds of interactions $V_{1,2}$. We find that when $V_1 \neq V_2$, or $V_1 = V_2$ and $J_\downarrow \neq J_\uparrow$, there is a gap

C. Solving the two-particle energy bands

We first consider only two particles with different spin in this system, as this can be easily solved and may shed light on some significant physics. The two-particle subspace can be spanned by the following basis:

$$\mathcal{H}^{(2)} = \{|r_\downarrow, r_\uparrow\rangle\}, \quad (19)$$

where r_\downarrow (r_\uparrow) refers to the position of a (b) particle. Considering lattice with $L_\downarrow = L_\uparrow = L$ sites, the dimension of the Hilbert space is L^2 .

According to Sec. II A, the eigenstates of a cotranslation operator under periodic boundary condition are found to be

$$|K, r_{\uparrow\downarrow}\rangle = \frac{1}{\sqrt{L}} \sum_{l=1}^N e^{iKl} |r_\downarrow + l, r_\uparrow + l\rangle, \quad (20)$$

where $r_\downarrow = r_\uparrow + r_{\uparrow\downarrow}$. To be explicit, we have used the notation $r_{\uparrow\downarrow}$ to label the eigenstates of cotranslation operator according to relative distance between two particles. This is a convenient way to distinguish the seed basis. As discussed in Sec. II A, the choice of r_\downarrow and r_\uparrow determines the gauge. In this calculation, we fix $r_\uparrow = 0$ and let $r_\downarrow = r_{\uparrow\downarrow}$. Then the seed basis used here are $\{|r_{\uparrow\downarrow}, 0\rangle\}$, $r_{\uparrow\downarrow} \in [-L/2, L/2]$.

The Bloch Hamiltonian can be derived from (18) as

$$H_{r'_{\uparrow\downarrow}, r_{\uparrow\downarrow}}(K) = \langle K, r'_{\uparrow\downarrow} | \hat{H} | K, r_{\uparrow\downarrow} \rangle, \quad (21)$$

which is an L -by- L matrix in the basis of $|K, r_{\uparrow\downarrow}\rangle$. For convenience, we arrange the basis in the order of $\{|K, r_{\uparrow\downarrow}\rangle\}$ by $r_{\uparrow\downarrow} = 1, 2, \dots, N/2 - 1, -N/2, -N/2 + 1, \dots, -1, 0$. In this manner, the matrix representation of $H(K)$ reads

between the isolated bands, as shown in Figs. 2(b) and 2(d), respectively. However, when $J_\downarrow = J_\uparrow$ and $V_1 = V_2$, the two isolated bands become gapless; see Fig. 2(c).

D. Topological nature of isolated bands

As pointed in the previous subsection, the system is the direct product of two simple lattices under interaction-free condition. It is already known that this system is completely topologically trivial. For strongly interacting condition, the two isolated bands are away from the continuum band. Since the two particles within the continuum band are quasi-independent, and the lattices are both trivial, the continuum states should also be trivial. It is more intriguing to explore the topological properties of isolated bands.

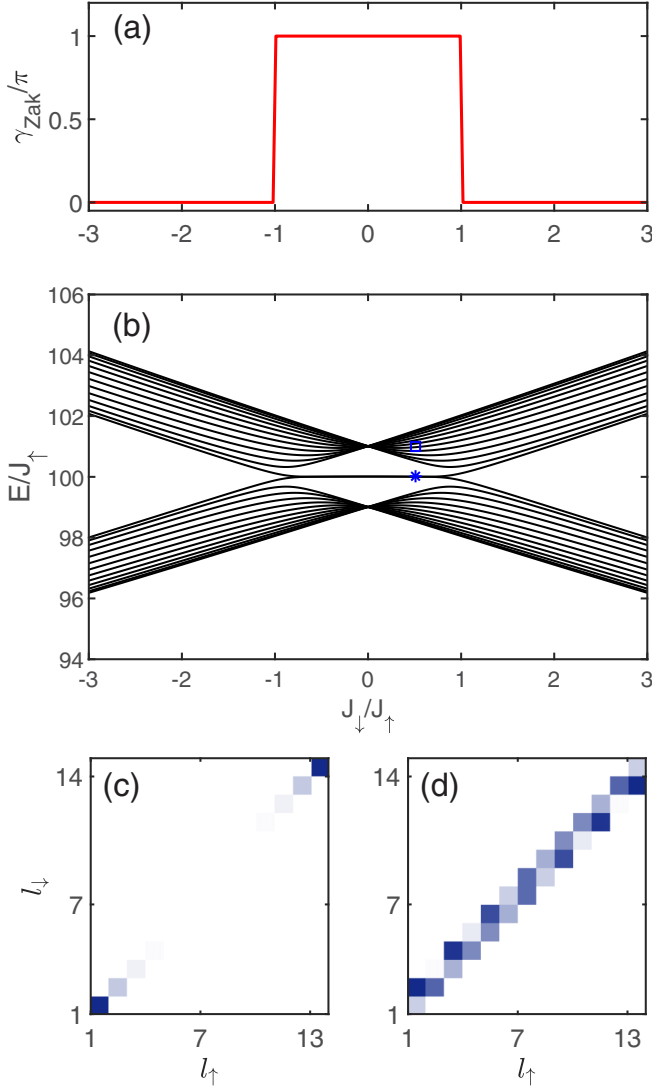


FIG. 3. (a) Zak phase of upper isolated band calculated vs $J_{\downarrow}/J_{\uparrow}$. (b) Eigenenergies of bound states vs $J_{\downarrow}/J_{\uparrow}$. The energy spectrum of scattering states are not shown here. Blue star and square respectively mark the in-gap bound states and the bulk bound states at $J_{\downarrow}/J_{\uparrow} = 1/2$, and their correlation matrices $\Gamma_{l,l'} = \langle n_{\downarrow,l} n_{\uparrow,l'} \rangle$ are shown in (c) and (d). The length of system is $L_{\downarrow} = L_{\uparrow} = 14$ for (a) with PBC and $L_{\downarrow} = 14, L_{\uparrow} = 13$ for (b)–(d) with symmetric OBC. The strength of interaction is set to $V = 100J_{\uparrow}$.

model shows a zigzag geometry, which still preserves the similar inversion symmetry.

2. Bulk-edge correspondence

Keeping $V_1 = V_2 = V$, we proceed to investigate the existence of topological edge bound states by imposing the open boundary condition (OBC). In fact, there are two different strategies to determine how the edge is terminated. One kind of OBC is that $L_{\downarrow} = L_{\uparrow}$, where the edge breaks the c.m. inversion symmetry, and we shall mention it by the *asymmetric boundary*. Another kind of OBC, mentioned by symmetric boundary, is that $L_{\downarrow} = L_{\uparrow} + 1$, which preserves the c.m. inversion symmetry. In the main text, we only consider

the symmetric boundary. For more discussions about these two kinds of terminations, see Appendix D.

By using exact diagonalization, we calculate the energy spectrum for different ratios of $J_{\downarrow}/J_{\uparrow}$ under the symmetric open boundary condition. We find that there are doubly degenerate in-gap states between the bulk of bound states only for $|J_{\downarrow}/J_{\uparrow}| < 1$, as shown in Fig. 3(b). Compared with Fig. 3(a), it is clear that this is in great agreement with the bulk topology discussed above. To uncover the properties of the in-gap bound states, we calculate the correlations of the two particles $\Gamma_{l,l'} = \langle n_{\downarrow,l} n_{\uparrow,l'} \rangle$. The correlation pattern shown in Fig. 3(c) clearly reveals the in-gap states are strongly localized and correlated, indicating the existence of edge bound states. For comparison, the bound states in bulk of band are highly delocalized but still bound together; see Fig. 3(d). The appearance and disappearance of in-gap bound states at edges is in agreement with our analysis in the bulk topology. As stated in Sec. II A, the c.m. Zak phase is related to the c.m. position of multiparticle Wannier states within a cell. Nontrivial Zak phase leads to extra density accumulation at the terminated edge if the edge is commensurate to the c.m. inversion symmetry. This phenomenon is usually called the bulk-edge correspondence [3,47].

III. INTERACTION-INDUCED THOULESS PUMPING

In this section, we would like to explore the topological pumping of bound states induced by the interaction effect. Recall that by adding modulation of on-site energy and tunneling, the SSH model is extended to the Rice-Mele model [49]. In the topological Thouless pumping scheme [2,50], the two distinct topological phases are connected through breaking the chiral (inversion) symmetry without closing the energy gap. After one period of pumping, the Zak phase winds for 2π , and the polarization is changed for a quanta. The Thouless pumping has already been realized experimentally and quantized particle-charge transport is observed [8,9].

For an interacting system, the topological pumping of two interacting bosons [22] and a many-body case [51,52] has been investigated. However, these interacting models have the topological single-particle counterpart in the interaction-free condition. Here, we propose a scheme to realize the quantized particle transport based on the interaction-induced topological bound states discussed in the previous section. In the same spirit of topological Thouless pumping, we add the modulations of both interaction and tunneling terms into our model, which are given as

$$\begin{aligned} \hat{H}_J(t) = & -[J - \delta(t)] \sum_l (\hat{c}_{\downarrow,l}^{\dagger} \hat{c}_{\downarrow,l+1} + \text{H.c.}) \\ & - [J + \delta(t)] \sum_l (\hat{c}_{\uparrow,l}^{\dagger} \hat{c}_{\uparrow,l+1} + \text{H.c.}), \end{aligned} \quad (29)$$

with $\delta(t) = \delta_0 \sin(\omega t + \varphi_0)$, and

$$\begin{aligned} \hat{H}_V(t) = & [V - \Delta(t)] \sum_l \hat{n}_{\downarrow,l} \hat{n}_{\uparrow,l} + [V + \Delta(t)] \\ & \times \sum_l \hat{n}_{\downarrow,l+1} \hat{n}_{\uparrow,l}, \end{aligned} \quad (30)$$

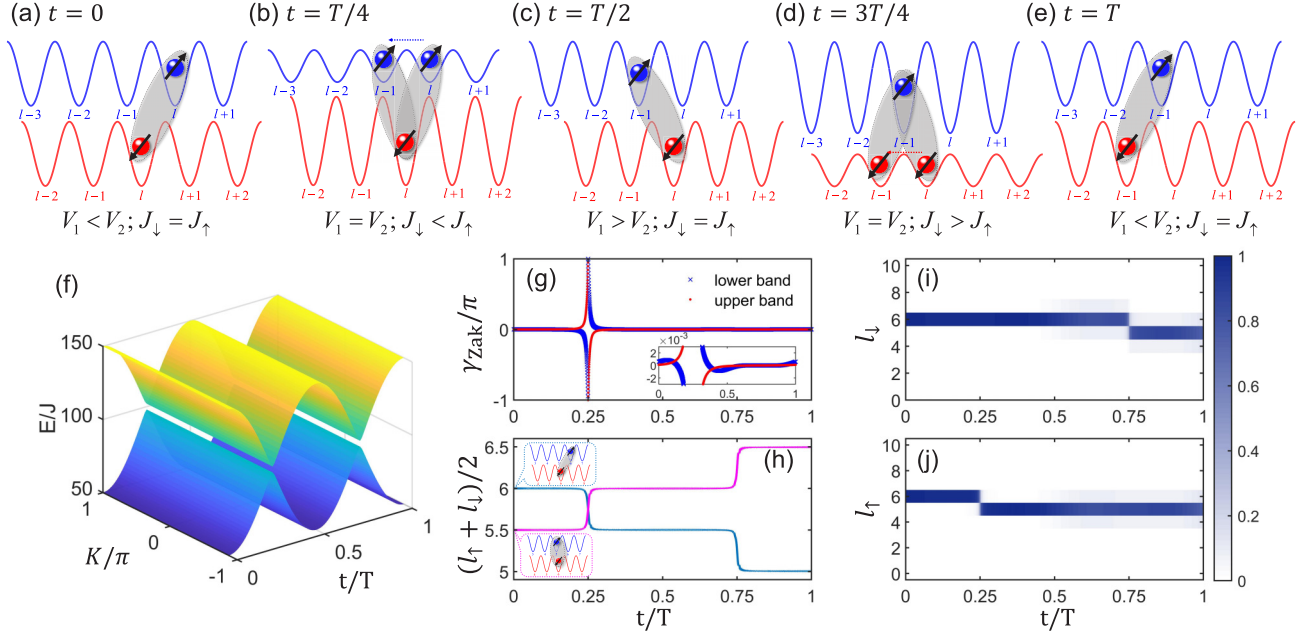


FIG. 4. Topological pumping of two-particle bound state in one period T . (a)–(e) Schematic illustrations of the pumping process. Red and blue lattices refer to periodic potentials for particle \downarrow and \uparrow , respectively. The bound state is formed as long as the interaction is strong enough. In (b) and (d), there appear degenerate states due to the equal strength of interaction $V_1 = V_2$. (f) A 3D view of bound-state energy bands in closed $K - t$ space of two-particle system. (g) The Zak phase γ_{Zak} of lower and upper isolated bands as a function of time t in a period. Inset shows an enlarged area around $\gamma_{\text{Zak}} = 0$. (h)–(j) Numerical simulation of two-particle topological pumping. Panel (h) shows a c.m. position shift of the two particles $l_{\text{c.m.}} = (l_{\downarrow} + l_{\uparrow})/2$ starting from two different initial states: $|\psi_{i_1}(0)\rangle = |6_{\downarrow}, 6_{\uparrow}\rangle$ (blue line) and $|\psi_{i_2}(0)\rangle = |6_{\downarrow}, 5_{\uparrow}\rangle$ (pink line). Insets show the schematic diagram of the two initial states. Panels (i) and (j) show density distributions of the two particles respectively during the pumping. For simplicity, we only show one of the results initialized as $|\psi_{i_1}\rangle = |6_{\downarrow}, 6_{\uparrow}\rangle$. Pumping parameters are chosen as $V = 100J$, $\Delta_0 = 50J$, $\delta_0 = J$ and $\omega = 3 \times 10^{-4}$, $\phi_0 = 0$. Lattice length is $L_{\downarrow} = L_{\uparrow} = 11$.

with $\Delta(t) = \Delta_0 \cos(\omega t + \phi_0)$. Here, δ_0 and Δ_0 are the modulation strengths of hopping and interactions, ω is the common modulation frequency, and ϕ_0 is the initial phase. The full modulated Hamiltonian is $\hat{H}(t) = \hat{H}_J(t) + \hat{H}_V(t)$. Experimentally, the modulation of tunneling can be realized through modulating the height of the periodic potential. For the modulation of interaction, it can be implemented by tuning the relative position of the two periodic potential [45], where the interaction is assumed to depend on the relative distance between particles. The demonstration of the pumping process is shown in Figs. 4(a)–4(e). Note that our pumping scheme is essentially different from the coherent transport using the state-dependent lattice in Ref. [45].

Under the PBC, our pumping scheme adiabatically connects two distinct topological phases of bound states via breaking the c.m. inversion symmetry without closing the gap. As shown in Sec. II A, the c.m. Zak phase indicates the c.m. position within a unit cell. After a pumping cycle, the Zak phase changes 2π and, correspondingly, the c.m. position of particles is shifted for a unit cell. This is also a useful approach to justify the topological nature. Considering $\phi_0 = 0$, $T = 2\pi/\omega$, the resonant tunneling between the two nearest-neighboring positions mainly occurs at $t = T/4$ and $t = 3T/4$ during the pumping cycle, which is protected by the nontrivial topology [53].

To ensure the existence of energy gap between isolated bands and continuum band, we focus on the regime that $|V \pm \Delta_0| \gg |J \pm \delta_0|$. The bound-state energy bands in a closed

$K - t$ space are shown in Fig. 4(f). According to Eq. (9), we calculate the Chern number of these two bands numerically, and the results are $C = \pm 1$ for upper and lower bands, respectively. We also calculate the Zak phase as a function of time in Fig. 4(g). With our choices of seed basis and the pumping parameters, the Zak phase will reach to π at $t = T/4$ and to 0 at $t = 3T/4$. At these two points, the system reduces to the model Eq. (18), and the Zak phase is strictly quantized. For other cases, the Zak phase is not quantized and will change with the parameters. The winding of Zak phase for each band matches the associated Chern number, coinciding with the following formula [39]:

$$C_n = \frac{1}{2\pi} \int_0^T dt \frac{\partial}{\partial t} \gamma_{\text{Zak}}^n(t). \quad (31)$$

Since the Zak phase is affected by the choice of seed basis and origin of unit cell [48,54], the results in Fig. 4(g) are not unique, and may vary with different choices [54]. However, the winding of Zak phase in Eq. (31) after a full pumping cycle is invariant and quantized [39,40,55].

As a verification of the topological pumping, we further simulate the quasiadiabatic pumping numerically. We shall start with two interacting particles in a nearest-neighboring site as an initial bound state: $|\psi_{i_1}(0)\rangle = |6_{\downarrow}, 6_{\uparrow}\rangle$ or $|\psi_{i_2}(0)\rangle = |6_{\downarrow}, 5_{\uparrow}\rangle$. These two kinds of initial bound states are dominated respectively by the two kinds of interaction V_1 and V_2 . During the adiabatic pumping, these two kinds of initial states will

evolve along lower or upper isolated bands accordingly. Thus the results of c.m. position shift will reflect the topology of the bands. The c.m. position of the particles during the time evolution is presented in Fig. 4(h). We also present the density distributions of particles initialized in $|\psi_{i_1}(0)\rangle = |6_\downarrow, 6_\uparrow\rangle$ during the pumping in Figs. 4(i) and 4(j). The results of numerical simulation show that the c.m. position of particles is shifted for one unit towards the left after a complete period. The change of c.m. position $(\Delta l_\downarrow + \Delta l_\uparrow)/2 = +1/-1$ is in agreement with the Chern number of upper or lower band.

IV. SUMMARY AND DISCUSSIONS

In summary, we have investigated the topological nature of interacting bound states and their transport in a state-dependent lattice. We find the existence of topological bound states protected by the c.m. inversion symmetry. This kind of symmetry requires the system should be invariant under the interchange of two kinds of distinguishable particles. The topological nature of bound states can be well characterized by the quantized c.m. Zak phase. As a result of bulk-edge correspondence, there appear topological edge bound states corresponding to nontrivial c.m. Zak phases. The repulsive bound pair can be regarded as the two-hole excitation of a filled attractively interacting system. Therefore, to some extent, the topological bound states reflect the topological excitations in an interacting many-body quantum system. Furthermore, the c.m. inversion symmetry in our system may suggest the possible existence of a symmetry-protected (SPT) phase [56] for the many-body ground state.

It should be noted that we assume no coherent population transfer between two internal states. This is essential for realizing the c.m. inversion symmetry. If there is such kind of population transfer, two particles become indistinguishable. Therefore, the c.m. inversion symmetry does no longer exist, since exchanging the relative position of two indistinguishable particles has no physical meaning. Without this essential symmetry, the Zak phase will no longer stay quantized. This means the coherent population transfer is a symmetry-breaking term.

On the other hand, we have also proposed a topological Thouless pumping via periodically modulating interaction and tunneling simultaneously. We obtain a nontrivial c.m. Chern number which is evidenced by the quantized shift of the c.m. position in the pumping process. Moreover, although both systems involve state-dependent lattices, our topological transport is different from the coherent transport via shifting the potential [45]. In our scheme, the periodic potential is assumed to shift back and forth, instead of shifting monotonously. The interplay between interaction and tunneling plays an important role during the pumping. In future, it would be intriguing to investigate the pumping of the ground state via the density matrix renormalization group or other techniques.

Our model may be realized in a current cold atoms experiment. The state-dependent optical lattice is an ideal platform [42,45] in which the interaction and tunneling are highly controllable. Besides, there are some other systems or techniques being the possible candidates for realizing the

interaction-induced topological bound states, such as the synthetic zigzag optical lattice [57,58]. We also note that our model is similar to that in Ref. [59], and therefore the experimental consideration may be shared.

ACKNOWLEDGMENTS

This work is supported by the Key-Area Research and Development Program of Guangdong Province under Grant No. 2019B030330001, the National Natural Science Foundation of China (NNSFC) under Grants No. 11874434 and No. 11574405, and the Science and Technology Program of Guangzhou (China) under Grant No. 201904020024. Y.K. was partially supported by the Office of China Postdoctoral Council under Grant No. 20180052 and the National Natural Science Foundation of China (NNSFC) under Grant No. 11904419.

APPENDIX A: STATE-DEPENDENT OPTICAL LATTICE

The state-dependent lattice has been widely used in a cold atoms experiment. The intraspecies interaction is used to control and produce the desired entanglement in quantum computation [43,60]. Usually, the state-dependent lattice consists of two σ^+ and σ^- polarized standing waves. Atoms with different internal states will be trapped by different standing waves. The Hamiltonian of a 1D state-dependent lattice with two bosonic components can be written in the language of second quantization

$$\hat{H} = \sum_{\sigma=\uparrow,\downarrow} \int dx \hat{\Psi}_\sigma^\dagger(x) \left[-\frac{\hbar^2}{2m} \nabla^2 + \mathcal{V}_\sigma^{\text{lat}}(x, \phi) \right] \hat{\Psi}_\sigma(x) + g_{\text{inter}} \int dx \hat{\Psi}_\uparrow^\dagger(x) \hat{\Psi}_\downarrow^\dagger(x) \hat{\Psi}_\uparrow(x) \hat{\Psi}_\downarrow(x), \quad (\text{A1})$$

where $\hat{\Psi}_\sigma$ is the field operator of spin- σ ($\sigma = \uparrow, \downarrow$) particle, $\mathcal{V}_\sigma^{\text{lat}}(x, \phi)$ is the state-dependent optical lattice potential, and $g_{\text{inter}} = 4\pi a_s \hbar^2/m$ is the interspecies coupling constant determined by s -wave scattering process. We have set the lattice constant to be $a = 1$. As we only consider the interspecies interaction in our model, the intraspecies interaction terms have been omitted. The state-dependent optical lattice potential can be written as

$$\begin{aligned} \mathcal{V}_\uparrow^{\text{lat}}(x, \phi) &= \mathcal{V}_\uparrow^{(0)} \cos^2(k_L x + \phi/2), \\ \mathcal{V}_\downarrow^{\text{lat}}(x, \phi) &= \mathcal{V}_\downarrow^{(0)} \cos^2(k_L x - \phi/2), \end{aligned} \quad (\text{A2})$$

where $\mathcal{V}_\sigma^{(0)}$ is the height of the lattice potential and ϕ is the relative phase shift of the lattice, which is affected by the laser polarization and can be controlled via the electro-optical modulator (EOM) experimentally [44,45,61].

With tight-binding approximation, one can expand the field operators in the 1D single-particle Wannier basis

$$\hat{\Psi}_\sigma(x) = \sum_l w_\sigma(x - x_l) \hat{c}_{\sigma,l}, \quad (\text{A3})$$

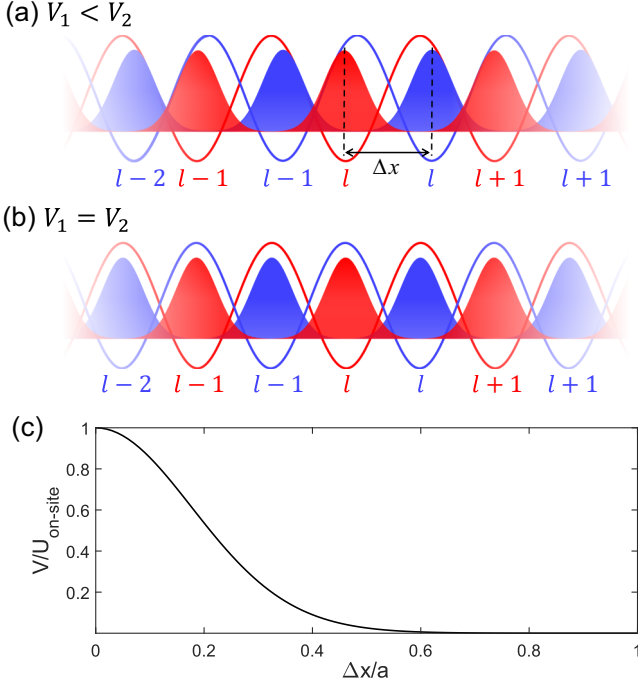


FIG. 5. Depiction for the intraspecies interaction in terms of the highly localized Wannier functions. Blue and red color respectively indicates the spin-up and spin-down particle and its associated trapping lattice. The interaction depends on the overlaps of the two Wannier functions, and we show two cases as a schematic illustration: (a) $V_1 < V_2$, corresponding to $a/2 < \Delta x < a$, and (b) $V_1 = V_2$, corresponding to $\Delta x = a/2$. Panel (c) shows the strength of interaction (in the unit of on-site interaction, which is the strongest) as a function of relative distance Δx between two Wannier functions. This result is based on the numerical calculation of the Wannier function of the lowest band with $\mathcal{V}_\sigma^{(0)} \approx 13E_R$.

where $w_\sigma(x - x_l)$ is the Wannier function of spin- σ particle localized around x_l . Finally, we obtain

$$\hat{H} = - \sum_{i,j,\sigma=\uparrow,\downarrow} J_{i,j}^\sigma \hat{c}_{\sigma,i}^\dagger \hat{c}_{\sigma,j} + \sum_{i,j,k,l} V_{i,j,k,l} \hat{c}_{\uparrow,i}^\dagger \hat{c}_{\downarrow,j}^\dagger \hat{c}_{\uparrow,k} \hat{c}_{\downarrow,l}, \quad (\text{A4})$$

where the tunneling and interaction energy are

$$J_{i,j}^\sigma = - \int dx w_\sigma^*(x - x_i) \left[-\frac{\hbar^2}{2m} \nabla^2 + \mathcal{V}_\sigma^{\text{lat}}(x) \right] w_\sigma(x - x_j),$$

$$V_{i,j,k,l} = g_{\text{inter}} \int dx w_\uparrow^*(x - x_i) w_\downarrow^*(x - x_j) w_\uparrow(x - x_k) \times w_\downarrow(x - x_l). \quad (\text{A5})$$

The strength of interspecies interaction depends on the overlap of Wannier functions, which is affected by their relative distance. The closer they are, the stronger they interact, as depicted in Figs. 5(a) and 5(b). Thus we are able to control the interspecies interaction via tuning the relative shift of the two lattices. The tunneling strength, on the other hand, may be engineered through the spin-dependent ac Stark shift [62].

The strengths of two NN interactions mentioned in main text read as

$$V_1 = \int dx |w_\uparrow(x - x_l)|^2 |w_\downarrow(x - x_l)|^2,$$

$$V_2 = \int dx |w_\uparrow(x - x_l)|^2 |w_\downarrow(x - x_{l+1})|^2. \quad (\text{A6})$$

Then we would like to estimate the strength of the NN interaction $V_{1,2}$. Generally, the NN interaction is omitted for a deep optical lattice, as it is very weak compared with the on-site interaction. However, the NN interaction considered in our model is quite different. If the relative phase between the two lattices is $\phi = \pi/4$ in Eq. (A2), the distance between two nearest Wannier functions of different species is $\Delta x = a/2$. In this condition, the integral of the interaction term in Eq. (A5) gives $V_1 = V_2$, corresponding to the case in our model. We numerically [63] calculate the integral Eq. (A5) for different relative distance Δx in Fig. 5(c). We find the NN interaction strength is roughly about $V_1 = V_2 \approx 0.025U_{\text{on-site}}$ when $\mathcal{V}_\sigma^{(0)} \approx 13E_R$. Here we use the on-site interaction $U_{\text{on-site}}$ for comparison. Usually, the ratio between on-site interaction U and NN tunneling J in optical lattice is in the magnitude of $U_{\text{on-site}}/J_{\text{NN}} \approx 36$ when $\mathcal{V}_\sigma^{(0)} \approx 13E_R$ for ^{87}Rb [64]. Thus the NN interaction strength is roughly about $V_1 = V_2 \approx 0.9J$, which is quite considerable. This estimation is in agreement with the result in Ref. [57], in which a similar type of interaction is considered. With the help of Feshbach resonance, it is possible to increase the s -wave scattering length and produce the desirable strong NN interaction. As shown in Fig. 5(c), the integral of interaction term in Eq. (A5) decays fast with the increase of distance. The interaction strength for $\Delta x = a$ is about $10^{-4}U_{\text{on-site}} \ll V_{1,2}$. Therefore, we may keep only the two NN interspecies interaction terms in our model (18).

APPENDIX B: EFFECT OF IMBALANCED INTERACTION ON ZAK PHASE

We briefly discuss if the two interactions are not equal, $V_1 \neq V_2$. In this case, the c.m. inversion symmetry would be broken and the relation in Eq. (23) does not hold. Hence the Zak phase is not quantized to 0 or π mode 2π , and will be affected by parameters. We calculate the Zak phase for different imbalance $\Delta V = (V_1 - V_2)/2$ in Fig. 6. One can note the nonzero Zak phase will decrease if the imbalance ΔV increases. This also explains why the Zak phase changes sharply in Fig. 4(g), since the imbalance of interaction strength is large for most time. If the imbalance is small $|\Delta V/J_{\downarrow,\uparrow}| \ll 1$, the Zak phase would still be close to 0 or π . It can be also noted that the effect of imbalance of the interaction in our model is in analogy to imbalance of the on-site potential of the sublattice in the SSH model, in which the chiral symmetry and inversion symmetry would be broken by this imbalance. To some extent, the considerations on such imbalance in these two models share some similarities.

APPENDIX C: EFFECTIVE MODEL FOR BOUND STATES

Taking the tunneling as perturbation, one can obtain the effective single-particle model describing the bound states.

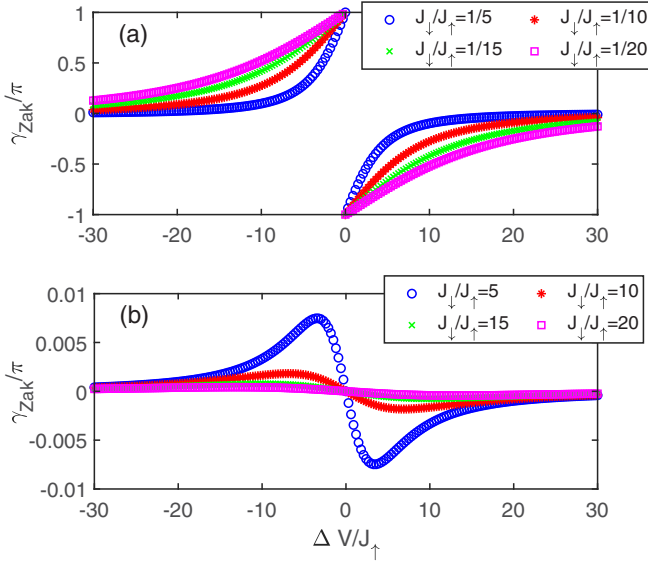


FIG. 6. Zak phase of upper isolated band vs different imbalanced interaction ΔV . Here $V_1 = V_0 + \Delta V$ and $V_2 = V_0 - \Delta V$ with $V_0 = 100J_\uparrow$; (a) and (b) show the results of $J_\downarrow < J_\uparrow$ and $J_\downarrow > J_\uparrow$, respectively. For simplicity, we only present the results of upper band.

For simplicity, we only consider the condition $V_1 = V_2 = V$. The unperturbed Hamiltonian reads

$$\hat{H}_0 = V \sum_l (\hat{n}_{\downarrow,l} \hat{n}_{\uparrow,l} + \hat{n}_{\downarrow,l+1} \hat{n}_{\uparrow,l}) \quad (\text{C1})$$

and the perturbative term is

$$\hat{H}_J = - \sum_{l,\sigma=\uparrow,\downarrow} (J_\sigma \hat{c}_{\sigma,l}^\dagger \hat{c}_{\sigma,l+1} + \text{H.c.}) \quad (\text{C2})$$

Aside from the eigenstates that two particles are separated, one can find two kinds of bound states $|d_{A,l}\rangle = c_{\downarrow,l}^\dagger c_{\uparrow,l}^\dagger |0\rangle =$

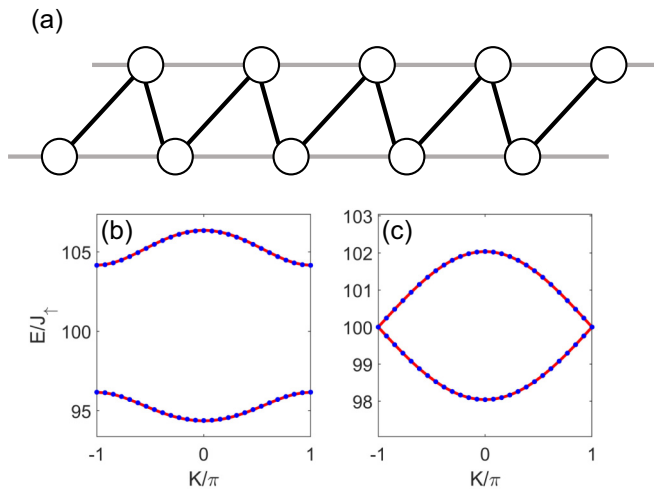


FIG. 7. (a) Lattice geometry of the effective model Eq. (C4). Black and gray lines represent first- and second-order effective tunneling of bound states. (b),(c) Comparison between original model and the effective single-particle model. Blue dots are calculated numerically from the original model and red lines are from the effective model. We set $J_\downarrow = 5J_\uparrow$ for (b), $J_\downarrow = J_\uparrow$ for (c), and $V_1 = V_2 = 100J_\uparrow$ for both.

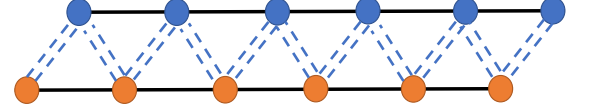
$|l_\downarrow, l_\uparrow\rangle$ and $|d_{B,l}\rangle = c_{\downarrow,l+1}^\dagger c_{\uparrow,l}^\dagger |0\rangle = |(l+1)_\downarrow, l_\uparrow\rangle$ with degenerate eigenenergy $E_0 = V$. By applying the degenerate perturbation theory up to second order [65],

$$\hat{H}_{\text{eff}} = E_0 \hat{P} + \hat{P} \hat{H}_J \hat{P} + \hat{P} \hat{H}_J \hat{S} \hat{H}_J \hat{P}, \quad (\text{C3})$$

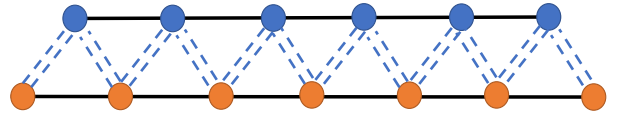
where $\hat{P} = \sum_l (|d_{A,l}\rangle \langle d_{A,l}| + |d_{B,l}\rangle \langle d_{B,l}|)$ is the projector onto the subspace spanned by unperturbed bound states and $\hat{S} = (\mathbf{1} - \hat{P})/V$ is a projector onto the orthogonal component of \hat{P} . Consequently, written in the form of particle operators, the effective Hamiltonian reads

$$\begin{aligned} \hat{H}_{\text{eff}} = & \left(V + \frac{J_\downarrow^2 + J_\uparrow^2}{V} \right) \sum_l (\hat{d}_{A,l}^\dagger \hat{d}_{A,l} + \hat{d}_{B,l}^\dagger \hat{d}_{B,l}) \\ & - \sum_l (J_\downarrow \hat{d}_{A,l}^\dagger \hat{d}_{B,l} + J_\uparrow \hat{d}_{B,l}^\dagger \hat{d}_{A,l+1} + \text{H.c.}) \\ & + \frac{J_\downarrow J_\uparrow}{V} \sum_i (\hat{d}_{A,i}^\dagger \hat{d}_{A,i+1} + \hat{d}_{B,i}^\dagger \hat{d}_{B,i+1} + \text{H.c.}). \end{aligned} \quad (\text{C4})$$

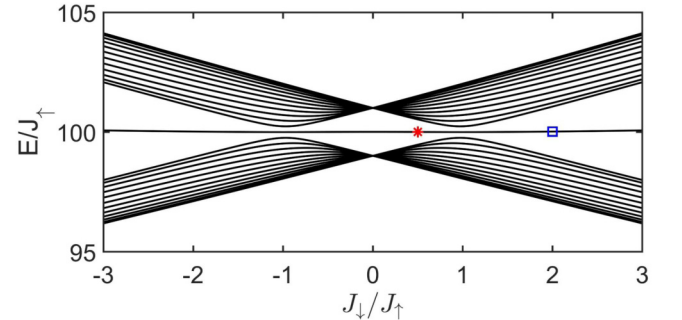
(a) asymmetric boundary



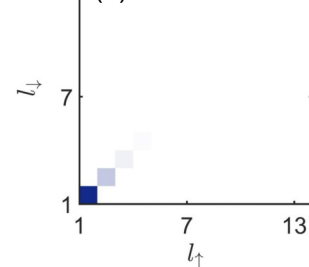
(b) symmetric boundary



(c)



(d)



(e)

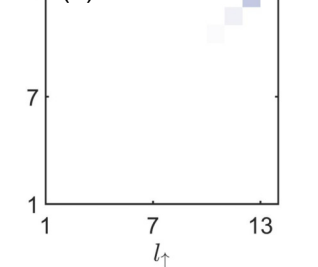


FIG. 8. (a),(b) Lattice geometry of the asymmetric and symmetric boundary. Blue-dashed lines indicate the interaction. (c) Eigenenergies of bound states vs J_\uparrow/J_\downarrow under the asymmetric-open boundary condition, with the same parameters as Fig. 3(a). (d),(e) The correlation matrices $\Gamma_{l,l'} = \langle n_{\downarrow,l} n_{\uparrow,l'} \rangle$ of the eigenstates correspond to red star and blue square in (c).

The first row in the above effective Hamiltonian is the homogeneous on-site energy. Second and third rows respectively correspond to dimerized NN tunneling and homogeneous next-nearest-neighbor (NNN) tunneling. This effective Hamiltonian indicates the zigzag geometry; see Fig. 7(a). The Fourier transformation yields

$$h(k) = d_0(k)I + d_x(k)\sigma_x + d_y(k)\sigma_y, \quad (\text{C5})$$

in which σ_i is the Pauli matrices, and $d_0(k) = V + (J_\uparrow^2 + J_\downarrow^2)/V + J_\downarrow J_\uparrow \cos(k)/V$, $d_x(k) = -J_\uparrow - J_\downarrow \cos(k)$, and $d_y(k) = -J_\downarrow \sin(k)$. It can be verified that the eigenenergy of this effective model coincides well with the original model up to the order of $O[(J_\downarrow + J_\uparrow)^3/V^2]$, as compared in Figs. 7(b) and 7(c). There is the inversion symmetry $\sigma_x h(k) \sigma_x = h(-k)$ and the Zak phase is quantized. In addition, it can be found that the inversion symmetry will be preserved for arbitrary order of perturbation. Such kind of property is due to the inversion-symmetric form of interaction and the tunneling does not break this symmetry.

APPENDIX D: ASYMMETRIC OPEN BOUNDARY CONDITION

The schematic diagrams of asymmetric and symmetric boundaries are shown in Figs. 8(a) and 8(b). We calculate the spectrum and in-gap states with an asymmetric boundary; see Figs. 8(c)–8(e). There is always an in-gap state, but the occupations on the edge are different. This can be understood from the effective model in Appendix C. With an asymmetric boundary, the effective lattice misses one site on the edge, and thus the two edges are in different dimerization. No matter how the ratio of $|J_\uparrow/J_\downarrow|$ changes, there will always an edge bound state if the lattice is long enough and the bulk-edge correspondence fails. The difference of the two kinds of termination as well as the results is because the bulk-edge correspondence should respect the symmetry that protects the topological properties [48,66]. In our model, the protecting symmetry is the c.m. inversion symmetry, which is broken by the asymmetric termination of the edge.

-
- [1] D. J. Thouless, M. Kohmoto, M. P. Nightingale, and M. den Nijs, Quantized Hall Conductance in a Two-Dimensional Periodic Potential, *Phys. Rev. Lett.* **49**, 405 (1982).
- [2] D. J. Thouless, Quantization of particle transport, *Phys. Rev. B* **27**, 6083 (1983).
- [3] M. Z. Hasan and C. L. Kane, Colloquium: Topological insulators, *Rev. Mod. Phys.* **82**, 3045 (2010).
- [4] C. L. Kane and E. J. Mele, Quantum Spin Hall Effect in Graphene, *Phys. Rev. Lett.* **95**, 226801 (2005).
- [5] F. D. M. Haldane, Model for a Quantum Hall Effect Without Landau Levels: Condensed-Matter Realization of the “Parity Anomaly”, *Phys. Rev. Lett.* **61**, 2015 (1988).
- [6] B. A. Bernevig and S.-C. Zhang, Quantum Spin Hall Effect, *Phys. Rev. Lett.* **96**, 106802 (2006).
- [7] B. A. Bernevig, T. L. Hughes, and S.-C. Zhang, Quantum spin Hall effect and topological phase transition in HgTe quantum wells, *Science* **314**, 1757 (2006).
- [8] M. Lohse, C. Schweizer, O. Zilberberg, M. Aidelsburger, and I. Bloch, A Thouless quantum pump with ultracold bosonic atoms in an optical superlattice, *Nat. Phys.* **12**, 350 (2016).
- [9] S. Nakajima, T. Tomita, S. Taie, T. Ichinose, H. Ozawa, L. Wang, M. Troyer, and Y. Takahashi, Topological Thouless pumping of ultracold fermions, *Nat. Phys.* **12**, 296 (2016).
- [10] M. Aidelsburger, M. Atala, M. Lohse, J. T. Barreiro, B. Paredes, and I. Bloch, Realization of the Hofstadter Hamiltonian with Ultracold Atoms in Optical Lattices, *Phys. Rev. Lett.* **111**, 185301 (2013).
- [11] G. Jotzu, M. Messer, R. Desbuquois, M. Lebrat, T. Uehlinger, D. Greif, and T. Esslinger, Experimental realization of the topological Haldane model with ultracold fermions, *Nature (London)* **515**, 237 (2014).
- [12] M. Atala, M. Aidelsburger, J. T. Barreiro, D. Abanin, T. Kitagawa, E. Demler, and I. Bloch, Direct measurement of the Zak phase in topological Bloch bands, *Nat. Phys.* **9**, 795 (2013).
- [13] E. J. Meier, F. A. An, A. Dauphin, M. Maffei, P. Massignan, T. L. Hughes, and B. Gadway, Observation of the topological Anderson insulator in disordered atomic wires, *Science* **362**, 929 (2018).
- [14] W. Sun, C.-R. Yi, B.-Z. Wang, W.-W. Zhang, B. C. Sanders, X.-T. Xu, Z.-Y. Wang, J. Schmiedmayer, Y. Deng, X.-J. Liu, S. Chen, and J.-W. Pan, Uncover Topology by Quantum Quench Dynamics, *Phys. Rev. Lett.* **121**, 250403 (2018).
- [15] L. W. Cheuk, A. T. Sommer, Z. Hadzibabic, T. Yefsah, W. S. Bakr, and M. W. Zwierlein, Spin-Injection Spectroscopy of a Spin-Orbit Coupled Fermi Gas, *Phys. Rev. Lett.* **109**, 095302 (2012).
- [16] Y.-J. Lin, K. Jiménez-García, and I. B. Spielman, Spin-orbit-coupled Bose-Einstein condensates, *Nature (London)* **471**, 83 (2011).
- [17] P. Wang, Z.-Q. Yu, Z. Fu, J. Miao, L. Huang, S. Chai, H. Zhai, and J. Zhang, Spin-Orbit Coupled Degenerate Fermi Gases, *Phys. Rev. Lett.* **109**, 095301 (2012).
- [18] J. Jünemann, A. Piga, S.-J. Ran, M. Lewenstein, M. Rizzi, and A. Bermudez, Exploring Interacting Topological Insulators with Ultracold Atoms: The Synthetic Creutz-Hubbard Model, *Phys. Rev. X* **7**, 031057 (2017).
- [19] N. R. Cooper, J. Dalibard, and I. B. Spielman, Topological bands for ultracold atoms, *Rev. Mod. Phys.* **91**, 015005 (2019).
- [20] S. de Léséleuc, V. Lienhard, P. Scholl, D. Barredo, S. Weber, N. Lang, H. P. Büchler, T. Lahaye, and A. Browaeys, Observation of a symmetry-protected topological phase of interacting bosons with Rydberg atoms, *Science* **365**, 775 (2019).
- [21] Q. Niu and D. J. Thouless, Quantised adiabatic charge transport in the presence of substrate disorder and many-body interaction, *J. Phys. A* **17**, 2453 (1984).
- [22] Y. Ke, X. Qin, Y. S. Kivshar, and C. Lee, Multiparticle Wannier states and Thouless pumping of interacting bosons, *Phys. Rev. A* **95**, 063630 (2017).
- [23] X. Qin, F. Mei, Y. Ke, L. Zhang, and C. Lee, Topological invariant and cotranslational symmetry in strongly interacting multi-magnon systems, *New J. Phys.* **20**, 013003 (2018).
- [24] R. Piil and K. Mølmer, Tunneling couplings in discrete lattices, single-particle band structure, and eigenstates of interacting atom pairs, *Phys. Rev. A* **76**, 023607 (2007).
- [25] M. Valiente and D. Petrosyan, Two-particle states in the Hubbard model, *J. Phys. B: At. Mol. Opt. Phys.* **41**, 161002 (2008).

- [26] J.-P. Nguenang and S. Flach, Fermionic bound states on a one-dimensional lattice, *Phys. Rev. A* **80**, 015601 (2009).
- [27] J. Javanainen, O. Odong, and J. C. Sanders, Dimer of two bosons in a one-dimensional optical lattice, *Phys. Rev. A* **81**, 043609 (2010).
- [28] K. Winkler, G. Thalhammer, F. Lang, R. Grimm, J. H. Denschlag, A. Daley, A. Kantian, H. Büchler, and P. Zoller, Repulsively bound atom pairs in an optical lattice, *Nature (London)* **441**, 853 (2006).
- [29] M. Di Liberto, A. Recati, I. Carusotto, and C. Menotti, Two-body physics in the Su-Schrieffer-Heeger model, *Phys. Rev. A* **94**, 062704 (2016).
- [30] M. A. Gorlach and A. N. Poddubny, Topological edge states of bound photon pairs, *Phys. Rev. A* **95**, 053866 (2017).
- [31] A. M. Marques and R. G. Dias, Multihole edge states in Su-Schrieffer-Heeger chains with interactions, *Phys. Rev. B* **95**, 115443 (2017).
- [32] A. M. Marques and R. G. Dias, Topological bound states in interacting Su-Schrieffer-Heeger rings, *J. Phys.: Condens. Matter* **30**, 305601 (2018).
- [33] X. Qin, F. Mei, Y. Ke, L. Zhang, and C. Lee, Topological magnon bound states in periodically modulated Heisenberg XXZ chains, *Phys. Rev. B* **96**, 195134 (2017).
- [34] G. Salerno, M. Di Liberto, C. Menotti, and I. Carusotto, Topological two-body bound states in the interacting Haldane model, *Phys. Rev. A* **97**, 013637 (2018).
- [35] H. Zhong, Z. Zhou, B. Zhu, Y. Ke, and C. Lee, Floquet bound states in a driven two-particle Bose-Hubbard model with an impurity, *Chin. Phys. Lett.* **34**, 070304 (2017).
- [36] E. Dobardžić, M. Dimitrijević, and M. V. Milovanović, Generalized Bloch theorem and topological characterization, *Phys. Rev. B* **91**, 125424 (2015).
- [37] J. Zak, Berry's Phase for Energy Bands in Solids, *Phys. Rev. Lett.* **62**, 2747 (1989).
- [38] J. Zak, Band Center—A Conserved Quantity in Solids, *Phys. Rev. Lett.* **48**, 359 (1982).
- [39] R. Resta, Macroscopic polarization in crystalline dielectrics: The geometric phase approach, *Rev. Mod. Phys.* **66**, 899 (1994).
- [40] W. A. Benalcazar, B. A. Bernevig, and T. L. Hughes, Electric multipole moments, topological multipole moment pumping, and chiral hinge states in crystalline insulators, *Phys. Rev. B* **96**, 245115 (2017).
- [41] R. Resta, Quantum-Mechanical Position Operator in Extended Systems, *Phys. Rev. Lett.* **80**, 1800 (1998).
- [42] D. Jaksch, H.-J. Briegel, J. I. Cirac, C. W. Gardiner, and P. Zoller, Entanglement of Atoms via Cold Controlled Collisions, *Phys. Rev. Lett.* **82**, 1975 (1999).
- [43] M. Olaf, G. Markus, W. Artur, R. Tim, T. W. Hänsch, and B. Immanuel, Controlled collisions for multi-particle entanglement of optically trapped atoms, *Nature (London)* **425**, 937 (2003).
- [44] B. Yang, H.-N. Dai, H. Sun, A. Reingruber, Z.-S. Yuan, and J.-W. Pan, Spin-dependent optical superlattice, *Phys. Rev. A* **96**, 011602(R) (2017).
- [45] O. Mandel, M. Greiner, A. Widera, T. Rom, T. W. Hänsch, and I. Bloch, Coherent Transport of Neutral Atoms in Spin-Dependent Optical Lattice Potentials, *Phys. Rev. Lett.* **91**, 010407 (2003).
- [46] M. Holland, S. J. J. M. F. Kokkelmans, M. L. Chiofalo, and R. Walser, Resonance Superfluidity in a Quantum Degenerate Fermi Gas, *Phys. Rev. Lett.* **87**, 120406 (2001).
- [47] T. Kariyado and Y. Hatsugai, Symmetry-protected quantization and bulk-edge correspondence of massless Dirac fermions: Application to the fermionic Shastry-Sutherland model, *Phys. Rev. B* **88**, 245126 (2013).
- [48] J.-W. Rhim, J. Behrends, and J. H. Bardarson, Bulk-boundary correspondence from the intercellular Zak phase, *Phys. Rev. B* **95**, 035421 (2017).
- [49] M. J. Rice and E. J. Mele, Elementary Excitations of a Linearly Conjugated Diatomic Polymer, *Phys. Rev. Lett.* **49**, 1455 (1982).
- [50] Q. Niu, Towards a Quantum Pump of Electric Charges, *Phys. Rev. Lett.* **64**, 1812 (1990).
- [51] E. Berg, M. Levin, and E. Altman, Quantized Pumping and Topology of the Phase Diagram for a System of Interacting Bosons, *Phys. Rev. Lett.* **106**, 110405 (2011).
- [52] A. Hayward, C. Schweizer, M. Lohse, M. Aidelsburger, and F. Heidrich-Meisner, Topological charge pumping in the interacting bosonic Rice-Mele model, *Phys. Rev. B* **98**, 245148 (2018).
- [53] D. Meidan, T. Micklitz, and P. W. Brouwer, Topological classification of adiabatic processes, *Phys. Rev. B* **84**, 195410 (2011).
- [54] H. Watanabe and M. Oshikawa, Inequivalent Berry Phases for the Bulk Polarization, *Phys. Rev. X* **8**, 021065 (2018).
- [55] R. D. King-Smith and D. Vanderbilt, Theory of polarization of crystalline solids, *Phys. Rev. B* **47**, 1651 (1993).
- [56] X.-G. Wen, Colloquium: Zoo of quantum-topological phases of matter, *Rev. Mod. Phys.* **89**, 041004 (2017).
- [57] E. Anisimovas, M. Račiūnas, C. Sträter, A. Eckardt, I. B. Spielman, and G. Juzeliūnas, Semisynthetic zigzag optical lattice for ultracold bosons, *Phys. Rev. A* **94**, 063632 (2016).
- [58] S. Greschner, L. Santos, and T. Vekua, Ultracold bosons in zigzag optical lattices, *Phys. Rev. A* **87**, 033609 (2013).
- [59] R. W. Chhajlany, P. R. Grzybowski, J. Stasińska, M. Lewenstein, and O. Dutta, Hidden String Order in a Hole Superconductor with Extended Correlated Hopping, *Phys. Rev. Lett.* **116**, 225303 (2016).
- [60] J. K. Pachos and P. L. Knight, Quantum Computation with a One-Dimensional Optical Lattice, *Phys. Rev. Lett.* **91**, 107902 (2003).
- [61] N. Belmechri, L. Förster, W. Alt, A. Widera, D. Meschede, and A. Alberti, Microwave control of atomic motional states in a spin-dependent optical lattice, *J. Phys. B: At. Mol. Opt. Phys.* **46**, 104006 (2013).
- [62] W. V. Liu, F. Wilczek, and P. Zoller, Spin-dependent Hubbard model and a quantum phase transition in cold atoms, *Phys. Rev. A* **70**, 033603 (2004).
- [63] K. Krutitsky, Ultracold bosons with short-range interaction in regular optical lattices, *Phys. Rep.* **607**, 1 (2016).
- [64] M. Greiner, O. Mandel, T. Esslinger, T. W. Hänsch, and I. Bloch, Quantum phase transition from a superfluid to a Mott insulator in a gas of ultracold atoms, *Nature (London)* **415**, 39 (2002).
- [65] M. Takahashi, Half-filled Hubbard model at low temperature, *J. Phys. C: Solid State Phys.* **10**, 1289 (1977).
- [66] J.-W. Rhim, J. H. Bardarson, and R.-J. Slager, Unified bulk-boundary correspondence for band insulators, *Phys. Rev. B* **97**, 115143 (2018).